Faraday rotation and polarization-modulated intense femtosecond laser pulses in a field-ionizing gaseous medium

C. X. Yu[1] and J. Liu[1,2,*]

[1]*National Laboratory of Science and Technology on Computational Physics, Institution of Applied Physics and Computational Mathematics, Beijing 100088, China*

[2]*Center for Applied Physics and Technology, Peking University, Beijing 100084, China*

(Received 24 June 2014; published 17 October 2014)

In this paper we investigate the propagation of an intense linearly polarized laser through an ionizing gaseous medium in the presence of an axial strong magnetic field, addressing the modulation of laser polarization. Our simulation indicates that the laser polarization can be dramatically modulated and shows complicated temporal patterns (Lissajous curves). This striking phenomenon can be attributed to the collective movement of ionized electrons, in contrast to the traditional Faraday rotation in which the rotation angle of the laser polarization derived from the linear response of the medium is time independent. We take the weighted average of the rotation angle over the whole pulse duration and find that it explicitly relies on strong magnetic strength as well as the incident laser intensity. Our finding has implications in strong magnetic diagnosis, laser intensity calibration, and the generation of polarization-modulated light sources.

DOI: 10.1103/PhysRevA.90.043834 PACS number(s): 42.25.Bs, 52.70.Ds, 32.80.Fb

I. INTRODUCTION

As a linearly polarized light propagates in a transparent medium for a distance with the assistance of an axial external magnetic field, its plane of polarization undergoes a rotation, known as Faraday rotation (FR) [1] or magneto-optical effect. The rotation angle can be evaluated by a simple formula $\theta = VBL$, where V is a frequency-dependent material parameter called the Verdet constant, L stands for the propagation distance, and B represents the magnetic strength.

Since its discovery and due to its unique form of relating the magnetic field to a rotation angle, FR had been regarded as the preferred method for diagnosing the strength of the magnetic field in many areas such as the galactic and interstellar magnetic fields [2], the megagauss or kilotesla magnetic fields in laser-produced plasmas (LPPs) [3–5], the magnetic-field structures in a laser-wakefield accelerator [6], and the real-time observation of laser-driven electron acceleration [7]. In the practical application fields, Faraday rotation also exhibits wide prospects such as optical isolators [8,9], magnetic-field sensors [10], current sensors [11,12], detection of biomagnetic fields [13], quantum memory [14], and many others [15–20].

A common interpretation for FR is that the incoming plane-polarized light splits into two opposite circularly polarized modes moving with different phase speeds. After propagating for a certain distance, a phase delay between the two modes indicates that the consequent light has a rotation with respect to the incoming one. As a matter of fact, the aforementioned FR originates in the linear responses of the transparent medium to the incident light, which corresponds closely to the collection of motions of bound electrons in the influence of an external axial magnetic field. Microscopically, the dynamics of an intra-atomic electron is modeled by a linearly harmonic potential. By collecting all the contributions from the intra-atomic electrons, one can obtain the linear polarization of the medium and calculate the difference between the linear refractive indices corresponding to the two opposite circularly polarized components, respectively, which determines their different phase speeds.

As the incident laser intensity increases, however, some nonlinear effects (say, Kerr effects and Raman effects, etc) become significant and should be taken into consideration, which ruins the simple linear relationship $\theta = VBL$ derived from the effective linear harmonic potential. In particular, as the laser intensity exceeds the ionization threshold and enters the tunneling regime, a considerable proportion of neutral atoms are ionized and a large number of laser-produced electrons contribute to the response of the medium. More importantly, the intense laser field leads to the time-varying densities of neutral atoms and plasmas, which means the time-varying refractive indices, and the external magnetic field changes the trajectories of ionized electrons. According to the classical electromagnetic theory, the electric field along the direction perpendicular to the incident polarized plane is excited by the electric current resulting from the electrons' motions [21]. It can be predicated that, for a sufficiently strong external magnetic field, there are no longer fixed phase delays between the two orthogonal components of the final electric field and the polarization of the final laser light would be twisted greatly with a certain chirality depending on the direction of the magnetic field.

The aim of the present research is twofold. On the one hand, in the presence of an axial strong magnetic field, we seek a parameter describing the polarizations of an intense laser penetrating into an ionizing gaseous medium. A potential application of our research is the interaction of an intense laser pulse with a dense plasma, which involves the self-generated magnetic field induced by the $\nabla n_e \times \nabla T_e$ mechanism [4,22], where n_e and T_e are the density and temperature distribution of the plasma, respectively. The generated magnetic field may exert an influence on the polarizations of incident laser pulse and consequently in turn affect the dynamics of the dense plasma. The generation and movement of ionized electrons are very sensitive to the intensity of the incident laser field. However, the measurement of the laser intensity has remained

*Corresponding author: liu_jie@iapcm.ac.cn

challenging for a long time and many schemes have been proposed both theoretically [23–25] and experimentally (see [26–28], and references therein). Our research may provide a probable scheme of diagnosing an ultrastrong magnetic field and calibrating the incident laser intensity. On the other hand, we present a method of generating the polarization-modulated intense laser pulse that can be utilized in the manipulation and control of chiral materials. Currently, an experimental scheme is proposed by using all-optically-induced transient metamaterials [29]. In their proposed scheme, the polarization of the trailing part is changed from linear to elliptical by manipulating the polarization of THz waveforms with subcycle switch-on times, in which the light absorption in the semiconductor causes the spatial density distribution of an electron-hole plasma and thus a refractive-index distribution in the slab.

To simplify the calculation and to reveal the mechanism for the twisted polarization of the laser pulse, our work remains confined to the atomic medium. This paper is organized as follows. Section II is devoted to the theoretical derivation of the propagation equation of an intense laser pulse in the presence of an axial intense magnetic field based on the Maxwell equations. In Secs. II A and II B we discuss separately the responses of the neutral atoms and LPPs to the laser field and present the propagation equation in Sec. II C. In Sec. III we perform numerical calculations for the propagation equation for several different incident laser intensities and magnetic strengths. A calibrating parameter that relates to the incident laser intensity and magnetic strengths is introduced in Sec. III B. In order to explore the mechanism underlying the rotation of laser polarization, we investigate the energy transfer and loss of the incident laser field in Sec. III C. Our results are summarized in Sec. IV.

II. THEORETICAL MODEL

Throughout this paper, the international system of units is adopted unless otherwise noted. The propagation of an intense laser pulse in an optical medium is completely modeled by the Maxwell equations. In order to describe the evolution of laser pulse along the **z** axis, we restrict our work to the comoving frame $\tau = t - z/c$ and $\xi = z$, where t and τ are the time variables of the laser pulse in the laboratory frame and comoving frame, respectively, ξ is the propagation variable, and c is the speed of light in a vacuum. Under the influence of a strong laser field, the medium can be ionized by tunneling mechanism. Using the slowly varying envelope approximation, the three-dimensional propagation of a strong femtosecond laser in a comoving frame is (see the Appendix)

$$-\frac{2}{c}\frac{\partial^2 \mathbf{E}(\xi,r_\perp,\tau)}{\partial\xi\partial\tau} + \nabla_\perp^2 \mathbf{E}(\xi,r_\perp,\tau) = \mu_0 \frac{\partial^2 \mathbf{P}_{\rm neu}(\xi,r_\perp,\tau)}{\partial\tau^2} + \mu_0 \frac{\partial^2 \mathbf{P}_{\rm ion}(\xi,r_\perp,\tau)}{\partial\tau^2}, \quad (1)$$

where $\nabla_\perp$ is the Laplace operator in the transverse plane and μ_0 is the magnetic permeability. The second term on the left-hand side of Eq. (1) stands for laser diffraction in the transverse plane. In the first term on the right-hand side (RHS), $\mathbf{P}_{\rm neu}$ represents the contribution of a neutral medium, which involves the dynamics of bound electrons under the influence of Coulomb attraction from nuclear cores and the external laser field. In the formalism of quantum mechanics, it is described by the transitions among energy levels, including the stimulated Raman scattering and stimulated Brillouin scattering. The second term $\mathbf{P}_{\rm ion}$ on the RHS is the contribution to the polarization from the LPP, which accounts for absorption due to optical-field ionization and plasma oscillations. For the sake of brevity, we denote the group of variables $(\xi,r_\perp,\tau)$ of macroscopic quantities, such as the electric field **E** and polarization **P**, by τ with no ambiguity.

A. Neutral atoms

For the convenience of introducing external magnetic fields, we start with the microscopic definition of polarization instead of the refractive index of the gaseous medium. According to classical electrodynamics, the corresponding macroscopic polarization of the neutral medium is characterized by the average deviations of the positive and negative charges,

$$\mathbf{P}_{\rm neu}(\tau) = eN_a(\tau)\mathbf{s}(\tau), \quad (2)$$

where $e = -|e|$ is the charge carried by an electron, $N_a(\tau)$ is the instantaneous neutral density, and $\mathbf{s}(\tau)$ is the displacement of intra-atomic electrons relative to their parent core.

From the classical point of view, the atomic electron in the ground state vibrates periodically around the nucleus in the absence of an external field, which is described by the Newtonian equation $\ddot{\mathbf{s}} = -\nabla V(s)$, where s is the relative position to the ionic core and the double dots mean the second derivative with respect to time. The potential $V(s)$ characterizes the interaction between the atomic electrons and the nuclear core. In this work we choose the harmonic potential $V(s) = \frac{1}{2}m_e\omega_0^2 s^2$ and omit the nonlinear effects of the gaseous medium on the influence of the intense laser field, which does not alter the conclusions obtained in this paper. Here m_e is the electron mass, ω_0 is the characteristic frequency of the intra-atomic electron, and s represents the deviation from the equilibrium position.

For a femtosecond infrared laser pulse, the distance traveled by an electron is far less than the wavelength of the laser pulse, which means that the electric dipole approximation (EDA) always holds. In the presence of a constant strong magnetic field $\mathbf{B} = B_0\mathbf{e}_\xi$ in the direction of the laser's propagation, the motion equation of a bound electron reads

$$m_e\frac{d^2\mathbf{s}(\tau)}{d\tau^2} + m_e\omega_0^2\mathbf{s}(\tau) = e\left[\mathbf{E}(\tau) + \frac{d\mathbf{s}(\tau)}{d\tau}\times\mathbf{e}_\xi B_0\right], \quad (3)$$

where the frequency $\omega_0 = I_p/\hbar$ to meet the harmonic motion of an electron orbiting around the ion, I_p is the ionization potential of an applied atom, and $\hbar$ is the reduced Planck constant. In the last term on the RHS, $\mathbf{e}_\xi$ is the unit vector in the direction of the laser's propagation. Because of the vector product of velocity $d\mathbf{s}/dt$ and magnetic field **B** in the last term on the RHS, Eq. (3) is a coupled differential equation. It is not easy to solve this equation analytically in the time domain. In order to avoid the introduction of an imaginary unit i, we solve it through direct numerical integration and calculate the macroscopic polarization from the neutral medium.

After obtaining the value of $\mathbf{s}(\tau)$ from Eq. (3), we can calculate the second derivative of Eq. (2) as

$$\frac{\partial^2 \mathbf{P}_{\rm neu}(\tau)}{\partial \tau^2} = e\frac{\partial^2}{\partial \tau^2}[N_a(\tau)\mathbf{s}(\tau)], \tag{4}$$

which is just the first term on the RHS of Eq. (1). Unlike the traditional model interpreting the Faraday rotation, this term accounts for the changes of neutral atoms with time. The varying neutral density $N_a(\tau)$ along the time τ is given below.

B. Plasma effects

For the femtosecond LPP, the EDA is still supposed to be valid. Because the electrons produced at different instances have different displacement relative to their parent ions, we need to treat their trajectories separately. The contributions from the electrons released at τ_0 to the polarization of the gaseous medium at τ are [30,31]

$$d\mathbf{P}_{\rm ion}(\tau) = e\mathbf{r}_{\tau_0}(\tau)dN_e(\tau_0), \tag{5}$$

where $\mathbf{r}_{\tau_0}(\tau)$ is the relative position vector of electrons to the parent ion. The electron density $N_e(\tau)$ is determined by the rate equation $dN_e(\tau)/d\tau = W(E)[N_0 - N_e(\tau)]$, where N_0 is the initial density of the gaseous medium. The ionization rate $W(E)$ depends on the ionization mechanisms parametrized by the electric strength E_0 through $\gamma_K = \omega_L\sqrt{2I_p}/E_0$ (in atomic units), where ω_L is the central angular frequency of the laser field, such as multiphoton ionization, tunneling ionization (TI), and over-barrier ionization (OBI).

Therefore, the total polarization at τ from the laser-ionized electrons can be obtained by integrating Eq. (5) over all the ionization instances $(-\infty,\tau]$,

$$\mathbf{P}_{\rm ion}(\tau) = \int_{-\infty}^{\tau} e\mathbf{r}_{\tau'}(\tau)\frac{\partial N_e(\tau')}{\partial \tau'}d\tau',$$

which involves all the contributions of the LPP and indicates the nonlocal characteristics of the electric field in the time domain.

The induced current $\mathbf{J}(\tau) = \partial\mathbf{P}_{\rm ion}(\tau)/\partial\tau$ is given by

$$\mathbf{J}(\tau) = e\mathbf{r}_{\tau}(\tau)\frac{\partial N_e(\tau)}{\partial \tau} + \int_{-\infty}^{\tau} e\frac{\partial \mathbf{r}_{\tau'}(\tau)}{\partial \tau}\frac{\partial N_e(\tau')}{\partial \tau'}d\tau', \tag{6}$$

where $\mathbf{r}_{\tau}(\tau) = I_p/eE(\tau)\mathbf{e}$ is the initial ionization position depending on the instantaneous electric strength. For a two-dimensionally polarized electric field, $\mathbf{E}(\tau) = E_x(\tau)\mathbf{e}_x + E_y(\tau)\mathbf{e}_y$, $\mathbf{e} = \mathbf{E}(\tau)/E$ is the unit vector in the direction of the electric field, where $E = |\mathbf{E}(\tau)|$, and $\mathbf{e}_x$ and $\mathbf{e}_y$ are the unit vectors along the preselected axes perpendicular to the laser's propagation. The first term on the RHS of Eq. (6) derives from the changes of the electron density relating to the ionization position.

In order to accomplish the derivation of Eq. (1), we calculate the second derivative of polarization with respect to τ as

$$\frac{\partial^2 \mathbf{P}_{\rm ion}(\tau)}{\partial \tau^2} = e\frac{\partial}{\partial \tau}\left[\mathbf{r}_{\tau}(\tau)\frac{\partial N_e(\tau)}{\partial \tau}\right] + e\frac{d\mathbf{r}_{\tau}(\tau)}{d\tau}\frac{\partial N_e(\tau)}{\partial \tau} + \int_{-\infty}^{\tau} e\frac{d^2\mathbf{r}_{\tau'}(\tau)}{d\tau^2}\frac{\partial N_e(\tau')}{\partial \tau'}d\tau'. \tag{7}$$

Here $d\mathbf{r}_{\tau}(\tau)/d\tau$ is the initial velocity of electrons when they are released. For a one-dimensional motion of electrons along the polarization of the laser field, the initial velocities are always supposed to be zero. When one considers a two-dimensional model transverse to the laser's propagation, however, the initial transversal velocities are supposed to satisfy a Maxwellian distribution. The factor $d^2\mathbf{r}_{\tau'}(\tau)/d\tau^2$ means the acceleration of electrons at τ under the influence of external fields.

The collisions of an electron with other electrons or atoms can be neglected due to the dilute gaseous medium. The dynamics of an electron that is created at τ_0 can be described by the Lorentz equation under the influence of a strong laser electric field $\mathbf{E}(\tau)$ and a strong magnetic field $\mathbf{B} = B_0\mathbf{e}_z$, which reads

$$m_e\frac{d\mathbf{v}_{\tau_0}(\tau)}{dt} = e[\mathbf{E}(\tau) + \mathbf{v}_{\tau_0}(\tau)\times\mathbf{e}_z B_0], \tag{8}$$

where the subscript τ_0 means the ionization instant. Here we omit the impact of the parent ion on an electron because the electron's trajectories are bent greatly by the external intense magnetic field and the Coulomb attraction from the parent ion can be neglected.

In order to obtain the analytical solution to Eq. (8), one can also write it in matrix form as

$$\frac{d\mathbf{V}_{\tau_0}(\tau)}{d\tau} = \mathbf{\Omega}\mathbf{V}_{\tau_0}(\tau) + \mathbf{F}(\tau), \tag{9}$$

where $\mathbf{\Omega} = \left[\begin{smallmatrix} 0 & \Omega_c \\ -\Omega_c & 0 \end{smallmatrix}\right]$ is a 2×2 matrix and $\Omega_c = eB_0/m_e$ is the electron cyclotron frequency (Larmor frequency) in the magnetic field B_0. The velocity matrix is represented by $\mathbf{V}_{\tau_0}(\tau) = [v^x_{\tau_0}(\tau)v^y_{\tau_0}(\tau)]^T$, where the superscripts x and y of $v^{x(y)}_{\tau_0}(\tau)$ mean the x and y components of the velocity vector of electrons released at τ_0, respectively, and the superscript T represents the matrix transposition. The inhomogeneous term on the RHS of Eq. (9) is $\mathbf{F}(\tau) = \frac{e}{m}[E_x(\tau)E_y(\tau)]^T$, which causes the accelerations of the ionized electrons.

Obviously, the matrix equation (9) is a kind of first-order ordinary differential equation, which can be solved analytically. Using the established procedure, one obtains its solution in terms of the integral form as

$$\mathbf{V}_{\tau_0}(\tau) = \exp[\mathbf{\Omega}(\tau-\tau_0)]\mathbf{V}_{\tau_0}(\tau_0) + \int_{\tau_0}^{\tau}\exp[\mathbf{\Omega}(\tau-\tau'')]\mathbf{F}(\tau'')d\tau''. \tag{10}$$

Since the exponential part of $\exp[\mathbf{\Omega}(\tau-\tau_0)]$ is a 2×2 matrix, Eq. (10) should be simplified in order to carry out our numerical calculations below.

In view of the expression of $\mathbf{\Omega}$, we introduce an antisymmetry matrix $\mathfrak{I} = \left[\begin{smallmatrix} 0 & 1 \\ -1 & 0 \end{smallmatrix}\right]$, which means $\mathbf{\Omega} = \mathfrak{I}\Omega_c$. It is easy to verify that $\mathfrak{I}$ has the properties

$$\mathfrak{I}^2 = -\mathbb{I}, \quad \mathfrak{I}^3 = -\mathfrak{I}, \quad \mathfrak{I}^4 = \mathbb{I},$$

where $\mathbb{I}$ denotes the 2×2 identity matrix. These properties mean that the introduced matrix $\mathfrak{I}$ behaves like the imaginary unit i. Therefore, using the properties of i, we can express the

exponential matrix $\exp[\mathbf{\Omega}(\tau-\tau_0)]$ as

$$\mathbf{M}(\tau,\tau_0)=\begin{bmatrix}\cos[\Omega_c(\tau-\tau_0)] & \sin[\Omega_c(\tau-\tau_0)]\\ -\sin[\Omega_c(\tau-\tau_0)] & \cos[\Omega_c(\tau-\tau_0)]\end{bmatrix}.$$

It is easy to verify that it has the properties

$$\mathbf{M}(\tau_0,\tau)=[\mathbf{M}(\tau,\tau_0)]^T,$$
$$\mathbf{M}(\tau_2,\tau_1)\mathbf{M}(\tau_1,\tau_0)=\mathbf{M}(\tau_2,\tau_0).$$

Evidently, the matrix $\mathbf{M}(\tau,\tau_0)$ acts like a rotation matrix, which rotates counterclockwise the velocity vector $\mathbf{V}_{\tau_0}(\tau)$ by an angle of $\theta=\Omega_c(\tau-\tau_0)$ within an interval $\Delta\tau=\tau-\tau_0$ because of the negative value of the electron charge e. Then one can rewrite Eq. (10) as

$$\mathbf{V}_{\tau_0}(\tau)=\mathbf{M}(\tau,\tau_0)\mathbf{V}_{\tau_0}(\tau_0)+\int_{\tau_0}^{\tau}\mathbf{M}(\tau,\tau')\mathbf{F}(\tau')d\tau'. \quad (11)$$

This illustrates that the Lorentz force from the magnetic field changes the electron trajectories with a frequency Ω_c, which generates the electron's velocity along the **y** axis. According to the classical Ampère-Maxwell equation [21], $\partial\mathbf{E}/\partial t\approx\mathbf{J}_s/\varepsilon_0$, the electric field in the direction of the **y** axis is excited, $\mathbf{J}_s$ is the electric current source caused by the plasma's motion in the driving laser field, ε_0 is the dielectric constant, and the generated magnetic field is neglected in the nonrelativistic regime.

C. Propagation equation

Finally, by substituting Eqs. (4) and (7) into Eq. (1) and using Eq. (8), we obtain the propagation equation of the laser pulse through a gaseous medium. In this paper it is not convenient to study the evolution of polarization of the incident laser pulse in the frequency domain. In order to avoid the introduction of the imaginary unit i from the time derivatives and to analyze the conversion of the electric field from the x component to the y component in the time domain, we integrate the two sides over time $(-\infty,\tau]$ and achieve the final equation in integro-differential form [30,31]

$$\frac{\partial\mathbf{E}}{\partial\xi}=\frac{c}{2}\nabla_\perp^2\int_{-\infty}^{\tau}d\tau'\mathbf{E}(\tau')-\frac{\mu_0 ec}{2}\frac{\partial}{\partial\tau}[N_a(\tau)\mathbf{s}(\tau)]-\frac{\mu_0 I_p c}{2}\left[\frac{1}{E(\tau)}\frac{\partial N_e(\tau)}{\partial\tau}\mathbf{e}\right]-\frac{e\mu_0 c}{2}\int_{-\infty}^{\tau}d\tau'\frac{\partial N_e(\tau')}{\partial\tau'}\mathbf{V}_{\tau'}(\tau')$$
$$-\frac{1}{2c}\int_{-\infty}^{\tau}d\tau'\omega_p^2(\tau')\mathbf{E}(\tau')-\frac{e^2\mu_0 c}{2m_e}B_0\int_{-\infty}^{\tau}d\tau'\left[\int_{-\infty}^{\tau'}\frac{\partial N_e(\tau'')}{\partial\tau''}\mathfrak{J}\mathbf{V}_{\tau''}(\tau')d\tau''\right], \quad (12)$$

where $\omega_p(\tau)=\sqrt{N_e(\tau)e^2/m_e\varepsilon_0}$ is the time-dependent plasma frequency due to the time-dependent electron density $N_e(\tau)$ and $\mu_0\varepsilon_0=1/c^2$ is used. The initial velocity of electrons $\mathbf{V}_{\tau'}(\tau')=d\mathbf{r}_\tau(\tau)/d\tau$ is to be determined below and the velocity vector (matrix) $\mathbf{V}_{\tau'}(\tau)$ is given by Eq. (11). In Eq. (12) the first term on the RHS is responsible for the transverse diffraction of the laser pulse and the second term shows that the laser pulse experiences a dispersion and absorption due to acceleration of the bound electrons in neutral atoms. The third term represents the laser loss due to the optical-field ionization of the gaseous medium. The last term on the first line on the RHS accounts for the production rates of electrons with a certain initial velocity perpendicular to the laser's polarization. Actually, this term contributes little to the process of the laser energy conversion because of the relatively small velocities in the tunneling regime and it can be dropped. The first term in the second line shows that the ionized electrons gain their kinetic energies from the laser field and excite the plasma oscillations with the time-varying frequency $\omega_p(\tau)$. The last term in the second line describes the bending of the electrons' velocity by the external strong magnetic field, which converts the laser energy from the x component to the y component, i.e., the excitation of the electric field along the **y** axis.

III. SIMULATIONS AND DISCUSSION

A. Numerical scheme

Calculations of the coupled integro-differential equation (12) in matrix form are numerically performed by means of the fourth-order Runge-Kutta approach for a laser pulse propagating in optical field-ionizing gaseous media. Since the refraction term has little influence on the evolution of the laser's polarization, we drop the first term on the RHS in order to reduce the consumption of machine time. Then the $(3+1)$-dimensional geometries reduce to a $(1+1)$-dimensional version. The first derivative of $[N_a(\tau)\mathbf{s}(\tau)]$ in the second term on the RHS is carried out utilizing the finite-difference method, which uses the five-point formula and has the accuracy of $O(\Delta\tau^4)$ with the step size $\Delta\tau$ [32]. Since we only consider the atomic ionization through a photoionization mechanism, the electron densities can be expressed as an analytical form and the first derivative of the electron density can also be given explicitly. Furthermore, the integration computation appearing on the RHS is performed using the cumulative trapezoidal numerical formalism.

The gases are prepared by helium atoms with a gas pressure $p=150$ Torr and a room temperature $T=300$ K, which allows us to approximate them as an ideal gas. According to the state equation of an ideal gas, we calculate the initial density $N_0\approx 4.8\times10^{18}$ cm^{-3} for the present parameters.

An incident laser pulse linearly polarized along the **x** axis with a central wavelength $\lambda_L=800$ nm is focused on the gaseous medium, which is expressed as

$$\mathbf{E}_{\rm in}(\tau)=\mathbf{e}_x E_0 f(\tau)\cos(\omega_L\tau+\phi_0),$$

where $\mathbf{e}_x$ is the unit vector along the x axis, the angular frequency $\omega_L=2\pi c/\lambda_L$, and the initial phase is set to be $\phi_0=0$ without loss of generality. The electric strength E_0 is an adjustable parameter relating to the laser intensity $I_0=\varepsilon_0 cE_0^2/2$. The envelop function $f(\tau)$ is supposed as a Gaussian shape, $f(\tau)=e^{-\tau^2/\tau_f^2}$, and τ_f characterizes the pulse length (the full width at half maximum of the intensity is then $\tau_{\rm FWHM}=\sqrt{2\ln 2}\tau_f$).

For the numerical calculation of Eq. (3), we adopt the predictor-corrector scheme with the initial position $\mathbf{s}_0$ and initial velocity $\mathbf{v}_0$ that satisfy the energy-conservation conditions (ECCs) $m_e v_0^2/2 + m_e\omega_0^2 s_0^2/2 = I_p$, where $s_0 = |\mathbf{s}_0|$ and $v_0 = |\mathbf{v}_0|$. The two-dimensional initial positions s_{x0} and s_{y0} uniformly distributed between $-\sqrt{2I_p/m_e\omega_0^2} \sim \sqrt{2I_p/m_e\omega_0^2}$ are achieved using the built-in random generator by Intel Visual Fortran (IVF), in which $s_0^2 = s_{x0}^2 + s_{y0}^2 \leqslant 2I_p/m_e\omega_0^2$ holds. Then the two-dimensional initial velocities v_{x0} and v_{y0} are obtained using the same procedure according to the ECCs.

Under the radiation of an intense laser pulse of the peak intensity $I_0 \sim 10^{15}$ W/cm^2, the helium gas experiences mainly the optical field ionization (TI or OBI depending on the Keldysh parameter γ_K), the evolution of the free-electron density is described by $N_e(\tau) = N_0\{1 - \exp[-\int_{-\infty}^{\tau} W(E)d\tau']\}$, and the neutral density is $N_a(\tau) = N_0 - N_e(\tau)$. Along with the values of the ionization rate $W(E)$ versus the electric field E obtained from Ref. [33], we obtain the ionization rate for an arbitrary electric field $E(\tau)$ by an interpolating fitting method, such as Lagrange interpolation.

To calculate the velocity of a laser-produced electron $\mathbf{V}_{\tau_0}(\tau_0)$ from Eq. (11), we need to assign its initial velocity $\mathbf{V}_{\tau_0}(\tau)$. In the adiabatic approximation, the initial velocities have a Gaussian-like distribution perpendicular to the instantaneous laser field and the longitudinal components along the instantaneous laser field are sufficiently small [34]. Therefore, the initial velocity of a tunneled electron is chosen to be $\mathbf{V}_{\tau_0}(\tau_0) \approx (0, \mathbf{V}_\perp)$ and the transverse velocity $V_\perp$ satisfies the distribution $f(V_\perp) = e^{-V_\perp^2\sqrt{2I_p}/|E(\tau_0)|}$ (in atomic units) [35]. When the instantaneous laser field polarizes at an angle θ to the $\mathbf{x}$ axis, as shown in Fig. 1, to ensure the zero longitudinal velocity $V_\parallel \sim 0$ and $V_\perp \sim |\mathbf{V}_{\tau_0}(\tau_0)|$, there must be

$$V_x \cos\theta + V_y \sin\theta = 0, \tag{13a}$$

$$(V_x \sin\theta)^2 + (V_y \cos\theta)^2 = (V_\perp \sin\phi_\xi)^2, \tag{13b}$$

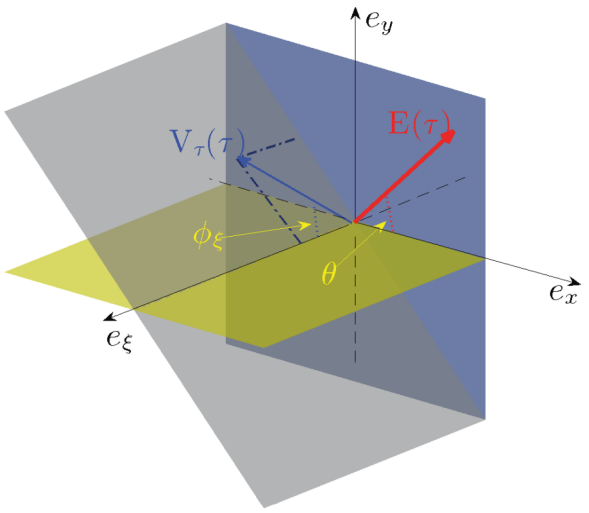

FIG. 1. (Color online) Diagram of the laser field and the initial velocity of an ionized electron. The laser field $\mathbf{E}(\tau)$ lies in the xy plane at an angle θ to the $\mathbf{x}$ axis and the initial velocity $\mathbf{V}_\perp$ lies in the plane perpendicular to the polarization of the electric field at a random angle ϕ_ξ to the ξ axis.

where ϕ_ξ is the angle between the propagation direction $\mathbf{e}_\xi$, V_x and V_y are the x and y components of the transversal velocity $\mathbf{V}_\perp$, respectively, and the angle θ is determined by computing $\tan\theta = E_y(\tau_0)/E_x(\tau_0)$. From Eqs. (13a) and (13b) we obtain

$$V_x = \pm\frac{V_\perp \sin\phi_\xi \sin\theta}{\sqrt{\sin^4\theta + \cos^4\theta}}, \quad V_y = \mp\frac{V_\perp \sin\phi_\xi \cos\theta}{\sqrt{\sin^4\theta + \cos^4\theta}}.$$

Here the value of $V_\perp$ obeys the Gaussian distribution $f(V_\perp)$ and the angle ϕ_ξ is distributed uniformly between 0 and 2π. Their values are both obtained using the built-in random generator by IVF.

B. Results and discussion

In our calculations, the computational time duration ranges from -10 to 20 fs considering the spreading of the laser pulse in the time domain. The number of grid points for τ is 1024, which corresponds to the grid spacing $\Delta\tau \approx 0.03$ fs. The incident laser intensity is $I_0 = 2.0 \times 10^{15}$ W/cm^2 with the width $\tau_f = 5.0$ fs and the external magnetic field is $B_0 = 1500$ T. We propagate the laser pulse for a distance of $\xi = 1.0$ cm with the fixed step size of $\Delta\xi = 0.1$ μm.

Figure 2 presents the profiles of the electric pulse propagating in the dilute helium medium for a distance of $\xi = 1$ cm. From Fig. 2(a) the electric field polarized along the $\mathbf{y}$ axis (marked by the green lines with stars) is generated and there is a time delay τ_{delay} between the leading peaks of the x and y

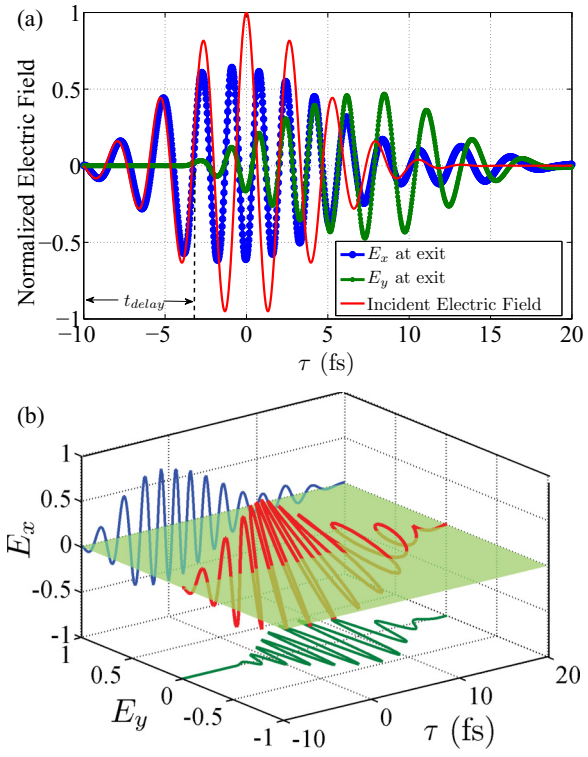

FIG. 2. (Color online) Profile of the output electric field at a distance of $\xi = 1$ cm: (a) the relative delay of the x and y components of the output electric field in the time domain and (b) the synthesized laser pulse (the zero plane is colored light green to intuitionally show the rotation of the laser polarization). Here the incident laser intensity is $I_0 = 2 \times 10^{15}$ W/cm^2 and the external magnetic strength $B_0 = 1500$ T.

components of the output electric field (OEF). For the purpose of facilitating a comparison, the incident laser pulse is also plotted using the red solid line. Evidently, from Fig. 2(a), the x component of the OEF denoted by the blue solid line with circles shifts its peaks and decays greatly, thus spreading as a long tail at the back edge of the pulse. The prior way causing the laser loss is the optical-field ionization, which occurs near the peaks of the laser. This is confirmed by the fact that the first two cycles of the incident laser satisfying $\gamma_K \gg 1$ are nearly unchanged during its propagation and the y component of the OEF (the green solid line with stars) is not created within the first two cycles.

In the third cycle, the peak strength of the driving laser reaches the TI threshold that satisfies the Keldysh criterion $\gamma_K \ll 1$ and the ionized electrons are produced dramatically due to the sufficiently strong electric field. With the assistance of an external magnetic field, the motion of the electrons is bent greatly according to Eq. (11), which excites the electric field along the **y** axis. It is noteworthy that the major part of the y component of the OEF appears between 5 and 10 fs. This is because the ionized electrons produced near the leading peaks gain their maximal velocity from the back edge of the incident laser pulse and the relative delay appears as a result. The simulations show that the most contributions to the excitation of the y component are made by the LPP in the dilute gaseous medium and the effects created by the neutral atoms are minimal. This also indicates that, for an intense light propagating through a dilute gaseous medium, the practical form of the atomic potential plays little or no role in the excitation of the laser field polarizing along the **y** axis.

In Fig. 2(b) we present the synthesized laser pulse from the x and y components of the OEF, which demonstrates intuitively the rotation of the laser's polarization through a light-green zero plane. During $\tau \in [-10,0]$ fs, the synthesized laser pulse basically polarizes along the **x** axis. While starting from 0 fs, i.e., at the front edge of the leading peak of the driving laser pulse, the polarization of the OEF rotates counterclockwise in the xy plane viewed from the front. In the trail of the OEF, it behaves like an elliptically polarized light.

In order to estimate the level of rotation of the laser polarization, we draw the Lissajous diagram for the OEF in polar coordinates, as illustrated in Fig. 3, where the radius represents the amplitude of the electric field. We can clearly see that the polarization mainly concentrates on the first and third quadrants. Therefore, seeking a parameter is useful to describe the relationships among the average deflection, the incident laser intensity and the strength of the external magnetic field. By weighting the angle $\theta(\tau)$ using the amplitude of the instantaneous electric field $E(\tau) = \sqrt{E_x^2(\tau) + E_y^2(\tau)}$, we can introduce a parameter $\langle\theta\rangle$, termed the average rotation angle (ARA), at a distance ξ as

$$\langle\theta\rangle = \frac{\int_{-\infty}^{+\infty} E(\tau)\theta(\tau)d\tau}{\int_{-\infty}^{+\infty} |E(\tau)|d\tau}, \tag{14}$$

where the rotation angle $\theta(\tau)$ is evaluated as the arc tangent of the ratio $E_y(\tau)/E_x(\tau)$. In Fig. 3, the ARA $\langle\theta\rangle \approx 16.89^\circ$ for the aforementioned parameters corresponds to the slope k of the blue dashed line with respect to the **x** axis through $k = \tan\langle\theta\rangle$.

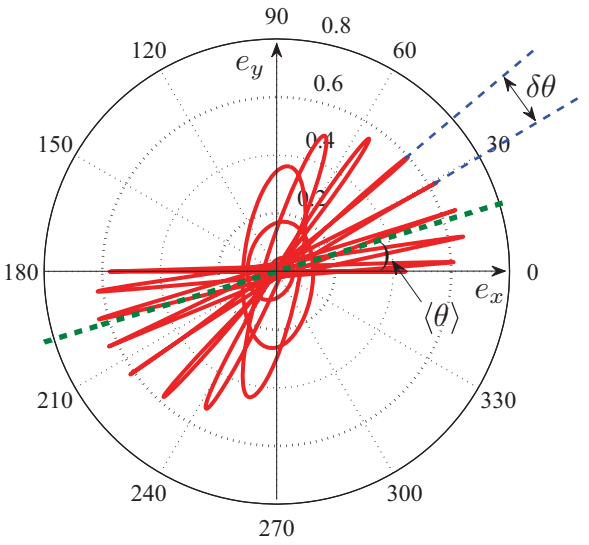

FIG. 3. (Color online) Lissajous diagram for the output laser pulse. The averaged rotation angle is calculated as $\langle\theta\rangle \approx 16.89^\circ$ and $\delta\theta \approx 12^\circ$ for the parameters $I_0 = 2.0 \times 10^{15}$ W/cm^2 and $B_0 =$ 1500 T. The slope of the green dashed line is given by $k = \tan\langle\theta\rangle$.

Different from the Faraday effects of a weak light that occurs in a transparent solid medium, such as fused silica, the polarization of an intense laser pulse propagating through a dilute gaseous medium for some distance undergoes a considerable variation within its pulse duration, as shown in Fig. 3. In this case, the rotation of the polarization plane of the laser pulse is evidently time dependent and we call it the instantaneous Faraday rotation (IFR). By definition, the Lissajous diagram records the polarization and magnitude of the laser field by eliminating the time at a fixed distance. Therefore, the angle $\langle\theta\rangle$ measures the deflection of the laser pulse under the influence of an external intense magnetic field. According to the analysis of the origin of $E_y(\tau)$ from Fig. 2, the ARA actually reflects the weighted average momentum and position distributions of ionized electrons by the ionization rates. Since the front edge of the laser pulse accounts for a considerable proportion in calculating the average rotation angle, as indicated in Fig. 2, the value of $\langle\theta\rangle$ is not as large as it appears.

From Fig. 3 we can also find an interesting phenomenon that the adjacent electric peaks in the first quadrant are separated by nearly equal angles that are denoted by $\delta\theta$. Moreover, we also notice from Fig. 2 that the relative time delays between the adjacent peaks are almost the same, where the electric field $E_x, E_y > 0$ corresponds to the first quadrant in Fig. 3. These facts allow us to introduce another parameter, i.e., the average rotating speed (ARS) $\overline{\omega} \approx \overline{\delta\theta/\delta\tau}$, where $\delta\tau$ stands for the relative time delay between the adjacent electric peaks for positive E_x and E_y and the mark $\overline{f}$ represents the effective fitted slope of the time-dependent curve $f(\tau)$. The term "effective" means that we only consider the cases with nonzero rotation angles and the larger electric peaks, as presented in Fig. 4. The black closed squares represent the electric peaks in the first quadrant in Fig. 3 and the blue pentagrams denote their rotation angles relative to the polarization plane of the incident laser pulse. It is clear that the significant rotation begins at

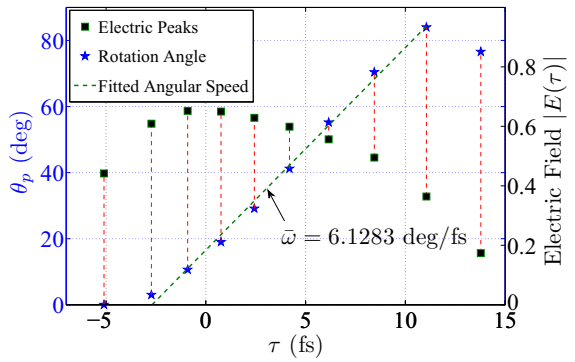

FIG. 4. (Color online) Electric peaks in the first quadrant and the corresponding rotation angle at the distance $\xi = 1$ cm for the parameters $I_0 = 2.0 \times 10^{15}$ W/cm^2 and $B_0 = 1500$ T. The slope of the green dashed line is given by $\overline{\omega} = 6.1283$ deg/fs.

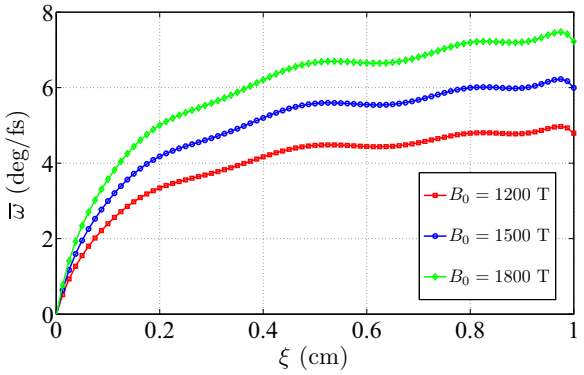

FIG. 6. (Color online) Rotating speeds of the laser polarized plane as functions of the distance ξ. Here the parameters are chosen as the incident laser intensity $I_0 = 2.0 \times 10^{15}$ W/cm^2 and the magnetic strength $B_0 = 1200$, 1500, and 1800 T.

about $\tau = -3$ fs, where the electric field E_y begins to appear, which can also be seen in Fig. 2(a). The effective rotation lasts until about $\tau = 8$ fs. By fitting and linear interpolation, we obtain the rotation speed $\overline{\omega}$ as the slope of the green dashed line. The parameter $\overline{\omega}$ demonstrates the ARS of the subsequent laser polarization, which depends on the amplitude of the external magnetic field through the collective movement of ionized electrons.

In order to trace out the evolution of the polarization of a laser field during its propagation in the dilute gaseous medium, we examine the ARA and the corresponding electron densities in the ionized channels in the wake of the elliptically polarized pulse for each propagation step. In Fig. 5 we plot the numerical results as functions of propagation distance, where the parameters of the laser field are the same as above and the magnetic strengths are chosen as 1200, 1500, and 1800 T, respectively, for comparison. Evidently, the densities of ionized electrons are almost the same for different magnetic fields, which means that the external magnetic field does not cause the extra energy loss of the laser field; this will be discussed below. During the laser pulse propagation for the distance of $\xi \lesssim 0.2$ cm, the ARA increases

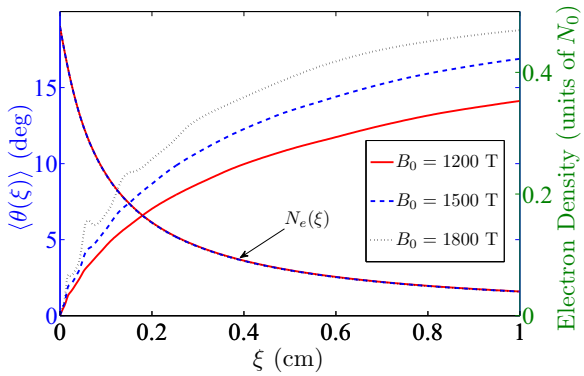

FIG. 5. (Color online) Evolution of the average rotation angle and the distribution of ionized electron density during the laser's propagation. It is clear that the densities of ionized electrons almost overlap for three different magnetic strengths. Here the incident laser intensity is $I_0 = 2.0 \times 10^{15}$ W/cm^2.

relatively rapidly because the strength of laser field is so strong that a large number of electrons are produced and participate in the creation of the electric field along the **y** axis. As the laser pulse continues propagating for a larger distance, the growth rates of the ARA become lower and lower due to the decay of the strength of the laser field and the consequent decrease of the electron densities. The results from three different magnetic strengths demonstrate that the stronger magnetic field is beneficial for the conversions between the two orthogonal polarizations of the laser pulse, which manifest as the higher average rotation angles (the black dotted line in Fig. 5).

In Fig. 6 we calculate the ARS for the polarization of the rear edge of the laser pulse during its propagation in the gaseous medium, where the same parameters are used as those in Fig. 5. As analyzed above, the IFR mainly originates from the collective movements of the ionized electrons, which indicates that the strong magnetic field can only exert a significant impact on the gaseous medium at the wake of the laser pulse. In fact, the parameter $\overline{\omega}$ reflects the influence of the magnetic field on the propagating laser pulse. It is clear from Fig. 6 that the stronger magnetic field leads to the higher rotating speed (the light green solid line with diamonds), which can be justified by the cyclotron motion of an ionized electron under the influence of the magnetic field with the cyclotron frequency $\Omega_c = |e|B_0/m_e$. It can be predicted that the maximum of the ARS does not exceed Ω_c. Therefore, the ARA $\langle\theta\rangle$ and the rotating speed of laser polarization $\overline{\omega}$ characterize the IRF of the incident laser pulse for two different aspects: The ARA emphasizes the pulse as a whole and the ARS mainly focuses on the fraction of the pulse with effective rotation.

In terms of probable experimental measurements, the ARA is more practical than the ARS. In order to explore the dependence of the ARA on the incident laser intensity and the external magnetic strength, we vary the peak laser intensity from 1.6×10^{15} and 2.2×10^{15} W/cm^2 by a spacing of 10^{14} W/cm^2 and the magnetic field B_0 from 100 to 2000 T by a spacing of 100 T, where the laser intensity $I_0 = 2.0 \times 10^{15}$ W/cm^2. The simulation results for the propagation distance of $\xi = 1$ cm are shown in Fig. 7 for the ARA of the OEF as functions of the magnetic magnitudes. We notice that the ARA exhibits a good linear dependence with respect to

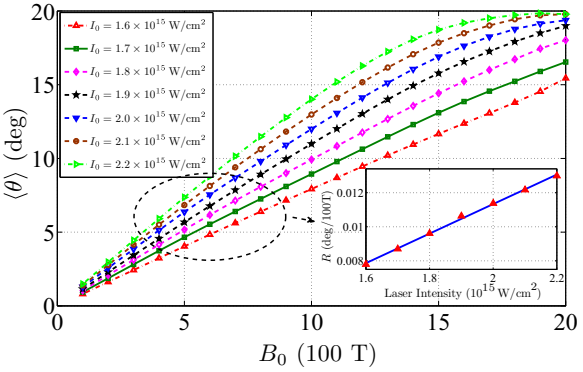

FIG. 7. (Color online) Average rotation angles as functions of different external strong magnetic fields for several incident laser intensities at the distance $\xi = 1$ cm. The inset shows the dependence of slope R on the incident laser intensity I_0, which also demonstrates good linearity.

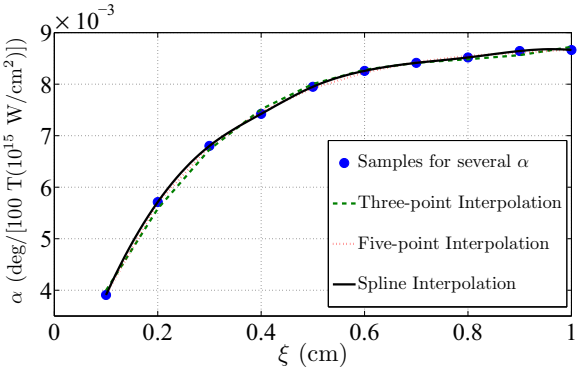

FIG. 8. (Color online) Values of α as functions of propagation distance ξ. The blue closed circles represent the sampling values calculated from the numerical simulations of the laser pulse.

the axial strong magnetic field. Therefore, we conclude that $\langle\theta\rangle = RB_0$ with an I_0-dependent coefficient $R = \alpha I_0$, where R stands for the slope of the curve describing the ARA as a function of the magnetic strengths and α is the slope of the blue line in the inset of Fig. 7. According to Fig. 5, for a fixed incident laser intensity and magnetic strength, the ARA is not a simple linear function of propagation distance. Therefore, the coefficient α is actually ξ dependent. Finally, we achieve an important expression

$$\langle\theta\rangle = \alpha(\xi) I_0 B_0. \tag{15}$$

In order to determine the coefficient $\alpha(\xi)$ based on the aforementioned temporal profiles of the incident laser pulse, we calculate its values for several distances of $\xi = 0.1, 0.2, \ldots, 1.0$ cm, respectively. Adopting a proper polynomial interpolation, we obtain its expression in the form of $\alpha(\xi) = \sum_{i=0}^{n} c_i \xi^i$, where n is the order of interpolation polynomials and c_i is the fitting coefficient, as given in Table I. For comparison, we also present the results from the spline interpolation; all of them are shown in Fig. 8.

It should be noted, however, that Eq. (15) has its scope. From Fig. 7, as the incident laser intensity reaches $I_0 = 2.2 \times 10^{15}$ W/cm^2 and the magnetic strength exceeds about 1600 T, the growth trend of the ARA slows down. This is because the stronger laser field causes the saturation of atomic ionizations and the two orthogonally polarized components of the laser field compete fiercely under the influence of a higher magnetic field through the cyclotron movements of ionized electrons. Consequently, the ARA eventually reaches its limits regardless of how strong the laser intensity and the magnetic field are. Moreover, for a higher magnetic field (such as $B_0 = 2000$ T), the validity of Eq. (15) is ensured by adopting a lower incident laser intensity.

The approximated linearity of the rotating angles of laser peaks with time allows us to introduce the ARS, which is an important parameter to characterize the modulation of the laser polarizations. As discussed and analyzed above, the rotation of the laser pulse is mainly caused by the collective motion of ionized electrons under the laser field and the external magnetic field for a tenuous gaseous medium. Therefore, the starting point of the rotation is sensitive to the incident laser intensity. In our calculations, the approximated linearity of rotation angle with time is still observed for several different laser intensities and magnetic strengths. In order to explore the dependence of the ARS on the incident laser intensity and magnetic strength, we calculate and fit the ARS according to the scheme plotted in Fig. 4. As shown in Fig. 9, the results at the distance of $\xi = 1$ cm also exhibit excellent linear relations of the ARS with the magnetic strength for lower incident laser intensities. In the inset of Fig. 9, the corresponding slopes $C_{\bar{\omega}}$ (red asterisks) depending on the incident laser intensity are presented, where the blue line represents the spline fitting. Similarly, for higher laser intensities and stronger magnetic fields, the linear relations are also broken.

TABLE I. Fitting coefficients of polynomial interpolations and orders $n = 3$ and 5, respectively.

n \ c_i	c_0	c_1	c_2	c_3	c_4	c_5
3	0.0019	0.0238	−0.0295	0.0125		
5	0.0010	0.0366	−0.0855	0.1158	−0.0842	0.0249

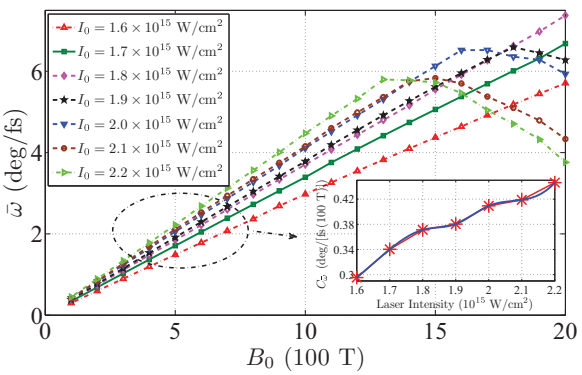

FIG. 9. (Color online) Dependence of the rotating speeds of the laser polarized plane on the incident laser intensity and magnetic strength at the distance $\xi = 1$ cm. The inset shows the slopes $C_{\bar{\omega}}$ depending on the incident laser intensity I_0. The spline fitting is represented by the blue line.

C. Energy conversion

As is well known, there is no exception that the underlying mechanism of all types of microscopic processes exhibits essentially the energy transfers and conversions. Based on the above analysis, the creation of the electric field along the **y** axis originates from the motion of ionized electrons along the **y** axis according to Maxwell's equations, in which the ionized electrons gain sufficient energy from the incident laser field. During the energy transfers and conversions, a great deal of energy is carried by ionized electrons in the form of their kinetic energy, which causes the heating of the partially ionized gaseous medium and the rapid loss of the laser field. Since the transverse refractions have been omitted during the laser's propagation, the statements of laser energy are represented by the energy density without confusion. Then the residual energies carried by the laser pulse are calculated as $P(\xi) = \int_{-\infty}^{+\infty} |\mathbf{E}(\xi,\tau)|^2 d\tau / P_0$, where $P_0 = \int_{-\infty}^{+\infty} E_{\rm in}^2(\tau) d\tau$ represents the incident laser energy with the strength of an incident laser field $E_{\rm in}(\tau)$.

According to classical electrodynamics, the force of the magnetic field always keeps perpendicular to the direction of the velocity and does not change the kinetic energy of the ionized electron. Therefore, the magnetic field causes the loss of laser energy and only transfers the laser energy between the two orthogonally polarized components, which will be discussed in the following section. To investigate the processes of energy transfer, we identify the laser energy by three destinations: the energy carried by the electric field polarized along the **x** and **y** axes, respectively, and the laser loss that causes the ionization of electrons, the heating of the gaseous medium, the generation of high-order harmonics, etc. For this purpose, we define the energy densities normalized to the incident laser pulse as

$$P_x(\xi) = \frac{1}{P_0}\int_{-\infty}^{+\infty} E_x^2(\xi,\tau) d\tau, \tag{16a}$$

$$P_y(\xi) = \frac{1}{P_0}\int_{-\infty}^{+\infty} E_y^2(\xi,\tau) d\tau, \tag{16b}$$

$$P_{\rm loss}(\xi) = 1 - P_x(\xi) - P_y(\xi), \tag{16c}$$

where $E_x(\xi,\tau)$ and $E_y(\xi,\tau)$ are the x and y components of the laser field at the distance ξ, respectively. Equation (16c) is defined by the energy-conservation law. The evolutions of different partitions of the laser energy are presented in Fig. 10.

As an incident laser pulse focuses on the gaseous medium, the atoms absorb sufficient energy to release their bound electrons by tunneling mechanisms and cause the loss of the driving laser pulse near the peaks. Then the ionized electrons are quiveringly driven by the laser field and external magnetic field. Some of their kinetic energy is converted into the electric field in the direction of their velocities according to Ampère's law, including in particular the one along the **y** axis, which causes the decline of the energy density of E_x (the red solid line) and the growth of the energy density of E_y (the blue dashed line), as shown in Fig. 10. The rest of the kinetic energy of ionized electrons and the ionization loss comprises of the laser loss (the black dash-dotted line).

To explore the dependence of energy partitions on the incident laser intensity and magnetic strength, we calculate

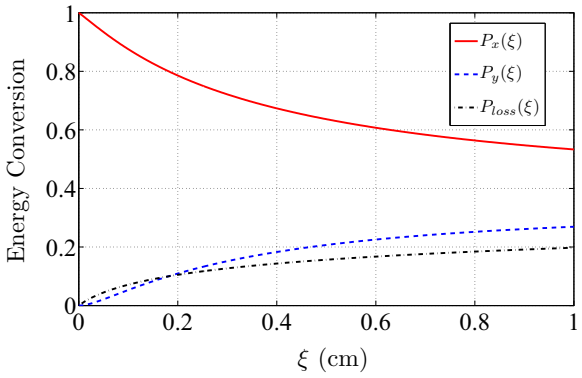

FIG. 10. (Color online) Evolution of different partitions of the laser energy during its propagation. The red solid line represents the evolution of the energy density of the x component of laser field and the blue dashed line represents that of the y component of the laser field. The parameters are $I_0 = 2.0 \times 10^{15}$ W/cm^2 and $B_0 = 1500$ T.

Eqs. (16a)–(16c) for different incident laser intensities and external magnetic strengths. In Fig. 11 we present the simulation results for a distance of $\xi = 1$ cm and the parameters used are given in the caption. The top panel shows the dependence of the energy conversion of E_x on the laser intensities and the magnetic strengths and the middle and bottom panels show P_y and $P_{\rm loss}$, respectively. We find that, for a stronger incident laser intensity or a stronger magnetic field, more energy of incident laser field is converted into the y components from x components. However, the laser loss by atomic ionization or heating of the medium is almost independent of the magnetic field and it only grows with increasing incident laser intensity, as shown in Fig. 11(c).

IV. CONCLUSION

Summarizing our theoretical results, we investigated an intense laser pulse propagating through a dilute gaseous medium under the influence of an external strong magnetic field. First, we derived the propagation equations satisfied

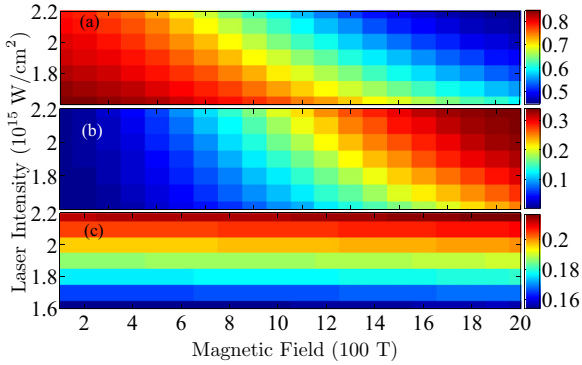

FIG. 11. (Color online) Dependence of energy transfer and conversion on the incident laser intensity and external magnetic strength. The laser intensity ranges between 1.6×10^{15} and 2.2×10^{15} W/cm^2 by a spacing of 10^{14} W/cm^2 and the magnetic strength varies from 100 to 2000 T by a spacing of 100 T, with the laser intensity $I_0 = 2.0 \times 10^{15}$ W/cm^2. (a) P_x, (b) P_y, and (c) $P_{\rm loss}$.

by the propagating laser pulse, during which we treated the response of the gaseous medium in two parts: the neutral atoms and the LPP. For the neutral response, we adopted a harmonic potential with an intrinsic frequency ω_0 chosen as the cyclotron frequency of an intra-atomic electron in the ground state. The treatment of responses from ionized electrons released at τ_0 were performed by analytically solving the Lorentz equations in matrix form and the initial velocities satisfied a Gaussian-like distribution weighted by the $E(\tau_0)$-based ionization rates. Then the numerical calculations were carried out by using the fourth-order Runge-Kutta approach and the derivatives of physical quantities with respect to time were evaluated by the five-point difference method.

The simulation results show that the irradiation of an intense incident laser field leads to significant ionizations of the gaseous medium, which means the time-varying densities of neutral atoms and ionized electrons. Due to the presence of the external intense magnetic field, an electric field polarized along the **y** axis is created with a relative time delay to the driving laser field. It is evident that the electric field $E_y(\tau)$ is generated only when the strength of the electric field enters the tunneling regime ($\gamma_K \ll 1$), which means that the ionized electrons play a dominant role in exciting the electric field $E_y(\tau)$. Because of the tenuity of the medium, the effect of neutral atoms on the excitation of electric fields polarized along the **y** axis can be neglected.

In order to evaluate the rotation of the polarization of the laser field, we defined two useful parameters, the average rotation angle $\langle\theta\rangle$ and the rotating speed $\overline{\omega}$, and analyzed their evolutions during the laser's propagation. By varying the incident laser intensities and the external magnetic strengths, we found that the average rotation angles keep increasing with the increasing initial laser intensity and external magnetic strengths for a fixed propagation distance. However, for a sufficiently intense laser intensity and external magnetic field, the average rotation angle reaches a limit because of the ionization saturation and the energy exchanges between the two orthogonally polarized components. By using polynomial fitting, we obtained a simple relation, i.e., Eq. (15), of the ARA with the propagation distance, the incident laser intensity, and the external axial magnetic field. Since the ARS is an important parameter to characterize the modulation of laser polarization, we investigated the dependence of the ARS on the incident laser intensity and the external magnetic field. The linear relations for the lower magnetic strengths and lower laser intensities were also demonstrated. Finally, we calculated the energy density normalized to the incident laser field and analyzed the processes of energy transfer and conversion of the laser field polarized along the **x** and **y** axes, respectively, and the loss caused by the ionizations and heating of the gaseous medium. The atoms first absorb sufficient energy from the incident laser field to release their electrons. Then ionized electrons continue gaining laser energy to obtain their kinetic energy and the external magnetic field bends its velocity, which creates the laser field polarized along the **y** axis according to Ampère's law.

From the analysis above, the polarization of the output electric field was determined by the incident laser field and the external magnetic field; it contains a wealth of information about the LPP. The chirality of the polarization plane of the output electric field depends on the direction of the axial magnetic field. A probable consideration of our work is in the interaction of a superstrong laser field with a dense plasma, where the self-generated magnetic field due to the density and temperature gradients of the plasma may exert an influence on the incident laser pulse. The obtained relation (15) implies a probable scheme for the diagnosis of the magnetic field and the calibration of laser intensity. Moreover, the flourishing research on the chiral materials has led to the demand for light sources with modulated polarization. In view of the potentially interesting applications of such polarization-modulated laser pulses, a great number of microscopic and macroscopic processes and the corresponding mechanisms are ongoing research issues. In order to produce the demanded polarization-modulated pulse for some special purposes, one needs to shape the profile of an incident laser pulse and adjust its initial intensity and the magnetic strength.

ACKNOWLEDGMENTS

This work was supported by the National Fundamental Research Program of China (Grants No. 2013CBA01502 and No. 2013CB834100), the National Natural Science Foundation of China (Grants No. 91021021 and No. 11274051), and a China Postdoctoral Science Foundation funded project (No. 2014M560920).

APPENDIX: DERIVATION OF EQ. (1)

Adopting the Coulomb gauge ($\nabla \cdot \mathbf{E} = 0$), the propagation of laser field in a medium is described by [21]

$$\nabla^2\mathbf{E} = \mu_0\frac{\partial^2\mathbf{D}}{\partial t^2} = \mu_0\varepsilon_0\frac{\partial^2\mathbf{E}}{\partial t^2} + \mu_0\frac{\partial^2\mathbf{P}}{\partial t^2}, \tag{A1}$$

where $\mathbf{D} = \varepsilon_0\mathbf{E} + \mathbf{P}$ is the electric displacement vector and the polarization $\mathbf{P} = \mathbf{P}_{\rm neu} + \mathbf{P}_{\rm ion}$ involves the contributions from neutral atoms and ionized electrons in the field-ionizing medium. In the comoving frame $\tau = t - z/c$ and $\xi = z$, which gives $\frac{\partial^2}{\partial\tau^2} = \frac{\partial^2}{\partial t^2}$ and $\frac{\partial^2}{\partial z^2} = \frac{\partial^2}{\partial\xi^2} - \frac{2}{c}\frac{\partial^2}{\partial\xi\partial\tau} + \frac{1}{c^2}\frac{\partial^2}{\partial\tau^2}$, Eq. (A1) becomes

$$\frac{\partial^2\mathbf{E}}{\partial\xi^2} - \frac{2}{c}\frac{\partial^2\mathbf{E}}{\partial\xi\,\partial\tau} + \nabla_\perp^2\mathbf{E} = \mu_0\frac{\partial^2\mathbf{P}_{\rm neu}}{\partial\tau^2} + \mu_0\frac{\partial^2\mathbf{P}_{\rm ion}}{\partial\tau^2},$$

where $\nabla^2 = \frac{\partial^2}{\partial z^2} + \nabla_\perp^2$ and $c^2 = 1/\mu_0\varepsilon_0$ are used. In a slowly varying envelope approximation [33,36,37], i.e., $\frac{\partial^2\mathbf{E}}{\partial\xi^2} \approx 0$, Eq. (1) is obtained.

[1] M. Faraday, Philos. Trans. R. Soc. London **136**, 1 (1846).
[2] S. A. Mao, B. M. Gaensler, M. Haverkorn, E. G. Zweibel, G. J. Madsen, N. M. McClure-Griffiths, A. Shukurov, and P. P. Kronberg, Astrophys. J. **714**, 1170 (2010).
[3] J. A. Stamper and B. H. Ripin, Phys. Rev. Lett. **34**, 138 (1975).
[4] J. A. Stamper, E. A. McLean, and B. H. Ripin, Phys. Rev. Lett. **40**, 1177 (1978).
[5] S. Fujioka *et al.*, Sci. Rep. **3**, 1170 (2013).

[6] M. C. Kaluza, H. P. Schlenvoigt, S. P. D. Mangles, A. G. R. Thomas, A. E. Dangor, H. Schwoerer, W. B. Mori, Z. Najmudin, and K. M. Krushelnick, Phys. Rev. Lett. **105**, 115002 (2010).
[7] A. Buck, M. Nicolai, K. Schmid, C. M. S. Sears, A. Sävert, J. M. Mikhailova, F. Krausz, M. C. Kaluza, and L. Veisz, Nat. Phys. **7**, 543 (2011).
[8] H. Takeda and S. John, Phys. Rev. A **78**, 023804 (2008).
[9] D. K. Efimkin and Yu. E. Lozovik, Phys. Rev. B **87**, 245416 (2013).
[10] D. Budker, D. F. Kimball, S. M. Rochester, V. V. Yashchuk, and M. Zolotorev, Phys. Rev. A **62**, 043403 (2000).
[11] A. H. Rose, M. N. Deeter, and G. W. Day, Opt. Lett. **18**, 1471 (1993).
[12] K. B. Rochford, A. H. Rose, M. N. Deeter, and G. W. Day, Opt. Lett. **19**, 1903 (1994).
[13] E. Bullmore and O. Sporns, Nat. Rev. Neurosci. **10**, 186 (2009).
[14] A. I. Lvovsky, B. C. Sanders, and W. Tittel, Nat. Photon. **3**, 706 (2009).
[15] M. L. Sadowski, G. Martinez, M. Potemski, C. Berger, and W. A. de Heer, Phys. Rev. Lett. **97**, 266405 (2006).
[16] S. G. Kaplan, S. Wu, H.-T. S. Lihn, H. D. Drew, Q. Li, D. B. Fenner, J. M. Phillips, and S. Y. Hou, Phys. Rev. Lett. **76**, 696 (1996).
[17] T. Morimoto, Y. Hatsugai, and H. Aoki, Phys. Rev. Lett. **103**, 116803 (2009).
[18] I. Crassee, J. Levallois, A. L. Walter, M. Ostler, A. Bostwick, E. Rotenberg, T. Seyller, D. van der Marel, and A. B. Kuzmenko, Nat. Phys. **7**, 48 (2011).
[19] A. V. Kimel, A. Kirilyuk, P. A. Usachev, R. V. Pisarev, A. M. Balbashov, and Th. Rasing, Nature (London) **435**, 655 (2005).
[20] V. Gasparian and Zh. S. Gevorkian, Phys. Rev. A **87**, 053807 (2013).
[21] J. D. Jackson, *Classical Electrodynamics*, 3rd ed. (Wiley, New York, 2001).
[22] J. A. Stamper, K. Papadopoulos, R. N. Sudan, S. O. Dean, E. A. McLean, and J. M. Dawson, Phys. Rev. Lett. **26**, 1012 (1971).
[23] H. G. Hetzheim and C. H. Keitel, Phys. Rev. Lett. **102**, 083003 (2009).
[24] D. F. Ye, G. G. Xin, J. Liu, and X. T. He, J. Phys. B **43**, 235601 (2010).
[25] H. Bauke, H. G. Hetzheim, G. R. Mocken, M. Ruf, and C. H. Keitel, Phys. Rev. A **83**, 063414 (2011).
[26] M. D. Perry, O. L. Landen, and A. Szöke, J. Opt. Soc. Am. B **6**, 344 (1989).
[27] A. S. Alnaser, X. M. Tong, T. Osipov, S. Voss, C. M. Maharjan, B. Shan, Z. Chang, and C. L. Cocke, Phys. Rev. A **70**, 023413 (2004).
[28] C. Smeenk, J. Z. Salvail, L. Arissian, P. B. Corkum, C. T. Hebeisen, and A. Staudte, Opt. Express **19**, 9336 (2011).
[29] N. Kamaraju, A. Rubano, L. Jian, S. Saha, T. Venkatesan, J. Nötzold, R. K. Campen, M. Wolf, and T. Kampfrath, Light: Sci. Appl. **3**, e155 (2014).
[30] C.-X. Yu, S.-B. Liu, X.-F. Shu, H.-Y. Song, and Z. Yang, Opt. Express **21**, 5413 (2013).
[31] C. X. Yu, S. B. Liu, X. F. Shu, H. Y. Song, and Z. Yang, Eur. Phys. J. D **67**, 90 (2013).
[32] T. Pang, *An Introduction to Computational Physics*, 2nd ed. (Cambridge University Press, Cambridge, 2006).
[33] A. Scrinzi, M. Geissler, and T. Brabec, Phys. Rev. Lett. **83**, 706 (1999).
[34] N. B. Delone and V. P. Krainov, J. Opt. Soc. Am. B **8**, 1207 (1991).
[35] J. Liu, Q. Z. Xia, J. F. Tao, and L. B. Fu, Phys. Rev. A **87**, 041403(R) (2013).
[36] I. P. Christov, Opt. Express **6**, 34 (2000).
[37] I. P. Christov, H. C. Kapteyn, and M. M. Murnane, Opt. Express **7**, 362 (2000).